Electrically Atomised Formulations of Timolol Maleate for Direct and On-Demand Ocular Lens Coatings

Prina Mehta[1], Ali Al-Kinani[2], Rita Haj-Ahmad[1], Muhammad Sohail Arshad[1], Ming-Wei Chang[3,4], Raid Alany G[2] and Zeeshan Ahmad[1*]

1. Leicester School of Pharmacy, De Montfort University, Leicester, LE1 9BH, UK
2. Kingston University London, School of Pharmacy and Chemistry, Kingston Upon Thames, KT1 2EE, Surrey, UK
3. College of Biomedical Engineering and Instrument Science, Zhejiang University, Hangzhou 310027, China
4. Zhejiang Provincial Key Laboratory of Cardio-Cerebral Vascular Detection Technology and Medicinal Effectiveness Appraisal, Zhejiang University, Hangzhou 310027, China

Corresponding author:
Prof. Z Ahmad: zahmad@dmu.ac.uk
Tel: +44 (0) 116 250 6455

Abstract

Advances in nanotechnology have enabled solutions for challenging drug delivery targets. While the eye presents numerous emerging opportunities for delivery, analysis and sensing; issues persist for conventional applications. This includes liquid phase formulation localisation on the ocular surface once administered as formulated eye-drops; with the vast majority of dosage (>90%) escaping from the administered site due to tear production and various drainage mechanisms. The work presented here demonstrates a single needle electrohydrodynamic (EHD) engineering process to nano-coat (as an on demand and controllable fiber depositing method) the surface of multiple contact lenses rendering formulations to be stationary on the lens and at the bio-interface. The coating process was operational based on ejected droplet charge and glaucoma drug timolol maleate (TM) was used to demonstrate surface coating optimisation, bio-surface permeation properties (flux, using a bovine model) and various kinetic models thereafter. Polymers PVP, PNIPAM and PVP:PNIPAM (50:50 %w/w) were used to encapsulate the active. Nano-fibrous and particulate samples were characterised using SEM, FTIR, DSC and TGA to confirm structural and thermal stability of surface coated formulations. More than 52% of nano-structured coatings (for all formulations) were <200nm in diameter. *In vitro* studies show coatings to exhibit biphasic release profiles; an initial burst release followed by sustained release; with TM-loaded PNIPAM coating releasing most drug after 24 hours (89.8%). Kinetic modelling (Higuchi, Korsmeyer-Peppas) was indicative of quasi-Fickian diffusion whilst biological evaluation demonstrates adequate ocular tolerability. Results from permeation studies indicate coated lenses are ideal to reduce dosing regimen, which in turn will reduce systemic drug absorption. Florescent microscopy demonstrated probe and probe embedded coating behaviour from lens surface *in vitro*. The multiple lens surface coating method demonstrates sustained drug release yielding promising results; suggesting both novel device and method to enhance drug activity at the eyes surface which will reduce formulation drainage.

Key Words: contact lens, fiber, drug delivery, timolol maleate, electrospinning, glaucoma

Introduction

Glaucoma is the 2nd leading cause of blindness in the world; affecting 2% of the worlds' population over 40 years of age [1]. It is a progressive multifactorial optic neuropathy, often resulting in vision loss due to heightened elevation in ocular pressure (OP). The increase in OP is a result of insufficient drainage of the aqueous humour (AH); (a transparent gel produced by the ciliary body in the eye which occupies the space between the cornea and lens). The reduction in removal of AH is due to anatomical changes in the trabecular meshwork. Here, the tubes which remove AH from the eye to the bloodstream are damaged which consequently lead to impairment of retinal nerves and the optic nerve [2]. At present, there is no cure for glaucoma and there is an urgent need to enhance the quality of life for patients and those currently on life-long treatment. Many of these regimens often require multiple dosing of active throughout the day.

Treatment of glaucoma is usually in the form of eye drops, a dosage form that makes up approximately 90% of all ocular formulations [3]. They are classed into those that reduce AH production (beta blockers, alpha agonists, carbonic anhydrase inhibitors) and those that improve the drainage of AH (prostaglandin analogues, cholinergics). Timolol (a beta adrenergic blocking agent) blocks the action of the sympathetic nervous system by competing with adrenergic neurotransmitters [4]. For the treatment of glaucoma, beta blockers like Timolol work by blocking the receptors in the ciliary body; reducing AH production [2]. However, Timolol also has an adverse effect on the cardiac and pulmonary system. If Timolol is present in the blood stream over a specific threshold concentration, it can slow down the heart rate, decrease blood pressure and reduce the function of the lungs, which can cause more inconveniences for the patient [4].

Despite ease of formulation and patient compliance, there are limitations with regards to the use of eye drops including nasolacrimal drainage and inability to control drug release leading to less than 5% of drug permeating through the cornea to targeting tissue; the ciliary body for glaucoma [5]. The biggest limitation is poor drug bioavailability as a result of short residence time in the eye. Consequently, to reach the therapeutic concentration in the eye, a higher dose of the drug needs to be administered [6]. Addressing these limitations has led to research being directed at the potential of various ocular devices; the most common

being soft contact lenses [7]. Contact lenses (CLs) are becoming increasingly common; replacing glasses for vision correction. However, recent developments have extended the use of CLs for cosmetics and therapeutics. The concept of using CLs as drug delivery devices was first introduced in the 1960's [8] but only in the last 2 decades have CLs been considered as useful ocular devices for delivery of drugs such as antibiotics [9], non-steroidal anti-inflammatory drugs (NSAIDs) [10], and anti-glaucoma actives [11,12]. Timolol (more specifically the maleate salt of Timolol (TM)) has been extensively used to assess the feasibility of CLs as drug delivery devices, with promising conclusions [13-15].

Many concepts, conventional and novel, to alter CLs and exploit the properties (e.g. the hydrophilicity [16]) of common hydrogel (HG) materials have been introduced to achieve sustained ocular drug delivery. Such notions include the simplicity of soaking lenses in a drug solution with consequent drug uptake in post-lens region (soak and release) [17] whilst more complex methods include molecular imprinting on HG matrix [18] or modifying the composition of the HG matrix [12]. Other methods involve embedding colloidal carriers (nanoparticles (NPs) [14], micelles [19]) within the HG matrix in an attempt to retard diffusion.

Electrohydrodynamic atomisation (EHDA) is a one-step deposition and an on demand method to coat biomaterials and is extendable to CLs. The principle revolves around using electrical forces to atomise liquids for the generation of nano and micrometre structures suitable for drug delivery. The fundamentals of this process are based on two vital processing parameters; applied voltage and flow rate. Various physical properties (viscosity, density and surface tension) also influence the resulting size and morphologies of the structures produced. This process is a versatile technique with great potential for enhancing bio-interfaces [20]. A large array of materials including temperature and stress sensitive active pharmaceutical ingredients (APIs)/materials (e.g. proteins and genes[21,22]) have been utilised to demonstrate the application of EHDA. Based on the choice of materials, it is possible to alter the release of drug when needed; in a controlled manner over minutes, hours or even days.

Since ocular formulation (liquid phase eye-drops) administration suffers loss from extensive drainage and tear forming mechanisms, the aim of this study was to develop an on demand

nano-structured multiple lens coating process; enabling greater formulation stability on lens surface and at the bio-interface. Polymers polyvinylpyrrolidone (PVP) and poly (N-isopropylacrylamide) (PNIPAM) were selected alongside glaucoma drug Timolol Maleate (TM) to optimise the multi-lens EHDA coating process. Formulation stability in matrix form was assessed using several techniques and the permeation (diffusive flux) across the bio-interface (cornea) was determined. *In vitro* release data was used to determine ideal kinetic models for TM release from various nano-structured systems on the lens coating. Fluorescent microscopy was also used to determine surface behaviour of both probe and probe-embedded lens coating *in vitro*.

Materials and Methods

Materials

PVP (4.4 x10^4 g/mol) was obtained from Ashland, UK. Methanol, PNIPAM (2-4x10^4 g/mol) timolol maleate (TM, ≥98%), acetone, sodium hydroxide and Rhodamine B were supplied by Sigma Aldrich, Dorset, UK. PureVision® (Balafilcon A) silicone hydrogel contact lenses manufactured by Bausch and Lomb (New York, USA) were utilised in this study. All reagents were of the analytical grade.

Solution Preparation

Polymeric solutions (selected polymer, or composite systems, at 5%w/v) containing TM (5% w/w of polymer) were prepared using methanol as the solvent by magnetic stirring for 10 minutes at ambient temperature (23°C). **Table 1** shows the composition of each formulation used.

Coating Application

A syringe containing 5mL of solution was attached to a syringe infusion pump (Harvard Apparatus, Pump 11-Elite, USA) which controlled the flow rate of polymer-drug solution. The solution was passed through silicone tubing which was connected to a stainless steel coaxial needle device (only single needle was utilised here, inner diameter 1.6mm) at various flow rates (5, 10 and 15 µL/min). The device was attached to a high power voltage supply (Glassman High Voltage Supply, UK). The electrically driven spraying process was

carried out at ambient temperature (23°C). Jetting mode-maps were constructed by varying the flow rate to optimise the processing parameters of the atomising system (**Figure 1a**).

Atomised coatings were deposited on microscope slides for preliminary analysis and subsequently onto commercial contact lenses. Pure Vision lenses were used in this study. For controlled deposition *via* atomised coatings, a lens holder device (accommodating up to 4 lenses) was built (**Figure 1b and 1c**), hosting ground electrodes, which enabled deposition onto peripheral regions of lenses whilst keeping the central regions un-coated (for sight). The lenses were weighted before and after to ascertain the mass of each coating. An illustration of the process mechanism is provided in **Figure 1d.** Exploratory experiments were performed to determine the spraying distance; as this is crucial in ensuring particle or fiber formation for thin film engineering.

Particle Coating Characterisation/analysis

Imaging

For preliminary studies coated microscope slides were analysed in detail using Scanning Electron Microscopy (SEM) to assess morphology of particle coatings. Prior to analysis, samples were gold coated (S150B, Edwards, Crawley, West Sussex, UK) under vacuum and images were obtained using a Zeiss Evo HD-15 (using an accelerating voltage of 5kV). Working distances between 9.5 and 10.5mm were utilised while applied voltages ranged from 10 to 18kV with magnifications of 5k and 50k; termed as low and high magnifications. Based on these results, the samples with the optimum conditions (uniform structures and near mono-dispersed particles) were further examined. These images were analysed using Smart Tiff software to obtain particle size distribution data. The optimised samples were observed at low magnification (x40) using Leica DME Optical Microscope using XL1 Camera Software. Digital images of uncoated and coated lenses with variable coating thickness were captured using a Samsung NX2000 Mirrorless digital Camera. Coating density was further confirmed using a Leica Model DM E-optical microscope. Probe encapsulation within engineered polymer particles was demonstrated using an EVOS Fluorescence Microscope at x40 magnification.

Thermal Analysis

The thermal properties of polymeric coating were analysed using Differential Scanning Calorimetry (DSC) and Thermogravimetric Analysis (TGA). DSC analysis was carried out using a Jade differential scanning calorimeter (Perkin Elmer, US). The DSC temperature scale of the DSC instrument was calibrated using indium as a standard; which has a known melting point of 156.6°C. Sealed pans containing 2-4mg of sample were heated under a flow of nitrogen gas at a rate of 20°C/min from 20 to 300°C. TGA analysis was carried out using Pyris 1 TGA thermogravimetric analyser (Perkin Elmer, US). Under the flow of nitrogen gas and air, sealed pans containing 8-10mg of sample were heated at a rate of 20°C/min from 20 to 700°C.

FTIR Spectroscopy

Potential interactions between drug (TM) and polymer were studied using Fourier Transform Infrared Spectroscopy (FTIR). Atomised samples, as well as neat materials, were scanned over the range 400-4000cm^{-1} using FTIR Platinum-ATR fitted with Bruker Alpha Opus 27 FT-IR at an average of 10 scans at resolution 4cm^{-1} at ambient temperature.

Contact Angle Analysis

Contact angle of the atomised structures were characterised using a ThetaLite TL100 contact angle goniometer; with data analysed using OneAttension software. 10µl distilled water droplets were used. Each sample was analysed 5 times in Sessile Drop mode and an average was obtained.

In vitro drug release studies

A lens holder was designed (for coated lenses) to enable surface contact between lens and the release medium; phosphate buffer saline (PBS) pH=7.4. The coated lenses were fixed in the holder and the whole device was placed into vials containing 10mL of PBS (at 37°C) which was constantly stirred. At predetermined time intervals, the holder was removed and placed into fresh PBS vials at 37°C. This method has been adapted from Mehta et al [27]. Drug release was determined using UV spectroscopy absorbance at λ=295nm. Collated *in vitro* release data were plotted in various kinetic models to evaluate the release kinetics of TM from the polymeric coatings.

In vitro probe release with fluorescent analysis

Using a similar set up described above for *in vitro* drug release, contact lenses were coated with various polymeric (PVP, PNIPAM, at 5%) and probe Rhodamine B (5 w/w% of polymer). The lenses were fixed into the lens holder and placed into vials of PBS at 37°C. Five lenses were coated and exposed to PBS for each polymer system and were removed from the vials at predetermined times (0 mins, 10mins, 1 hr, 6 hrs and 24 hrs). Experiments were performed in triplicate for both polymers. Fluorescent microscopy was used to determine dye intensity on the lens and UV Spectroscopy (λ=560nm) was used to exhibit dye intensity (DI) in the release medium.

Biological evaluation of TM-Loaded Nano-structures

To assess the ocular tolerability of various formulations; a Bovine Corneal Opacity and Permeability (BCOP) test was carried out. The BCOP test is an evaluation of ocular irritation caused by the test formulation; specifically interference with the corneal integrity. The three test samples were evaluated as well as normal saline for a negative control, sodium hydroxide (NaOH) as a positive control and acetone for mild positive control. Freshly excised bovine eyes were assessed for any corneal damage and undamaged eyes were subsequently incubated for 10 minutes at 37±0.5°C in a water bath. One drop of normal saline solution was introduced to the bovine cornea, before further incubation (5 mins). 100µL of the sample was administered onto the corneal surface and was left for 30 seconds. The bovine eye was washed with 10mL of normal saline and was incubated for an additional 10 mins. Any corneal damage to the cornea was assessed visually by gauging the extent/degree of opacification sample was carried out as well as a staining method, using sodium fluorescein solution (2%w/v) under a cobalt blue light (465-490nm).

Ex vivo corneal permeation of TM

Corneal permeation of TM was assessed using Franz diffusion cells with diffusional surface area of 1.77cm^2 (steps taken shown in **Figure 1e**). Freshly excised bovine eyes were evaluated for any damage before being carefully dissected to remove the entire cornea with a 2mm sclera ring to maintain cornea integrity. Cornea's were rinsed with PBS and placed between the donor and receptor compartments, with the endothelium facing the receptor

compartment (which was filled with 12 mL PBS and a mini stirrer). The Franz cells were maintained at 35±0.5°C. $00µL of sample was removed at predetermined intervals and replaced with 400µL fresh PBS. UV spectroscopy (λ=295nm) was used to analyse samples. The cumulative amount of drug permeating through the cornea was plotted as a function of time. The slope of the linear portion of the graph was calculated. This rate of release was divided by the diffusional area to determine steady state flux, shown in **Equation 1**:

$$J_{ss} = \frac{\left(\frac{dM}{dt}\right)}{A} \qquad \textbf{(Eq.1)}$$

Where J_{ss} is steady state flux ($\mu g.cm^{-2}.h^{-1}$), dM/dt is the rate and *A* is the area available for diffusion. Apparent permeability coefficient was calculated by dividing flux by donor concentration of TM, as shown in **Equation 2**:

$$P_{app} = \frac{J_{ss}}{C_d} \qquad \textbf{(Eq.2)}$$

Where P_{app} is the apparent permeability coefficient ($cm^2.s^{-1}$), C_d is the TM concentration in donor compartment.

Statistical Analysis

All experiments (unless stated) were carried out in triplicate. Statistical analysis (one-way analysis of variance, ANOVA) was performed. Differences in results between formulations were considered significant at a level of $p<0.05$.

Results and Discussion

In this study, PVP was used to demonstrate rapid drug release from a polymeric coating and encapsulation system. It is a common pharmaceutical excipient with good biocompatibility. PNIPAM is a biocompatible [23] temperature-sensitive polymer which undergoes reversible phase transition where it transforms from swollen state to dehydrated state (≥32°C). At physiological temperature, PNIPAM can expel its contents (losing up to ~90% of its original weight); rendering it useful in controlled drug delivery in the human body.

Electrohydrodynamic atomisation of formulations

Figure 2 shows a conductive (no liquid, no applied voltage (**Figure 2a**)) needle/nozzle alongside formulation F1 in dripping mode which arises due to an incremental rise in applied voltage (**Figure 2b**). Stable EHDA jets for formulations are shown in **Figures 2c-e** (F1, F2 and F3, respectively). There are various EHDA spraying modes characterised based on 2 principles; i) how the liquid jet leaves the conducting needle and ii) how the liquid jet breaks up. Dripping mode (**Figure 2b**) arises when fragments rather than droplet emerge from the needle. Jetting mode is observed when liquid breaks up into fine droplets, forming a stable Taylor cone (a prerequisite for controllable, near-uniform particle production) [24] at the nozzle exit, as seen in **Figures 2c-e**. Jetting mode-maps (**Figure 2f-h**) for each formulation show process optimisation windows at which stable jets are formed; ensuring production of near-monodispersed atomised droplets which undergo rapid drying to form nano-structures (particles, fibers or beaded fibers). Due to polymeric formulations possessing different physical liquid properties (based on selected polymer and solvent system), processing parameters (applied voltage, flow rate) need to be optimised to achieve samples of near-monodispersed diameter size distribution. Each solution was subject to flow rates ranging from 0 to 20µL/min, to determine the optimum voltage using 1µL/min increments. With respect to formulations F1, F2 and F3, an applied voltage between 13 and 20kV sufficed for stable jet production, yielding atomised structures within the nano-meter range in the form of particle and beaded structures; all of which are characteristic of EHDA engineering. The deposition distance is an important factor in the EHDA process. Exploratory experiments were performed to determine an ideal deposition (needle tip to substrate) distance for particle engineering. This was determined to be 12cm.

Imaging

Figures 3a-c show images of uncoated and coated contact lenses. **Figure 3a** displays a blank, uncoated lens. **Figures 3b** and **3c** display fine and coarse coatings, respectively. The density of coatings was also analysed using optical microscopy at x40 magnification as seen in **Figures 3d-e**. The presence and morphology of the resulting particles were identified using SEM at x5k and x50k magnification (**Figures 3g-l**). The most spherical, uniform particles were produced using F1 at a flow rate of 15µL/min. A comparison between stable formulation coating deposition show fibrous structures are obtained for F2 (10µL/min) and F3 (10µL/min). The difference in structural morphology arises due to the increased viscosity of

parent formulations once PNIPAM was incorporated. The appearance of well-defined particles and fibres show the TM-loaded structures were essentially dry before depositing on the collection plate. This also suggests the vast majority of the vehicle (methanol) successfully evaporated from atomised formulations during the process. However, formulations F2 and F3 show collapsed/porous particles, although defined, indicating the evaporation rate of the solvent from the droplets (forming particles or fibers) to be rapid [25]. **Figures 3m-o** shows the entrapment of probe within the polymeric nano-structures. **Figure 3m** shows the encapsulation of Rhodamine B in PVP matrix, showing a green hue. **Figures 3n** and **3o** correspond to the fluorescence images showing encapsulation of probe Rhodamine B. Fluorescence imaging demonstrated encapsulation of probe within nano-structure polymeric matrix. Excitation of the C=O bond in PVP polymer emitted a longer wavelength (green). The conjugated double bonds within the ring structure in Rhodamine B induced red-shift in absorption when exposed to RFP. The composite structures appear yellow; demonstrating probe encapsulation within PVP nano-structures (**Figure 3m**). PNIPAM does not fluoresce; hence when overlaid with Rhodamine B micrographs under RFP a speckled effect is observed (**Figure n**). **Figure 3o** shows images for composite particles. Yellow structures can be seen due to the presence of PVP in the formulation.

Particle and fiber size analysis

Using Smart Tiff software, data was collated to reveal particle size distribution (PSD) of atomised structures. **Figure 4** shows the PSD for formulations F1, F2 and F3, each signifying positively skewed data. . This indicates that more than ~50% of NPs produced were between 1-200nm in diameter. The mean diameter was 183, 262 and 458nm for F1, F2 and F3, respectively. This increase in mean diameter is due to production of fibrous structures in formulations that contained PNIPAM. Increased solution viscosity leads to the generation of fibrous and spherical structures being produced, often termed beaded, which arise due to a transition between spraying (particles) and spinning (fibers). In this instance, mean diameters appear larger. Despite this, <2% of atomised particles were more than 1µm in diameter. These findings coincide with previous studies which used PVP as a polymeric matrix. Rasekh et al produced indomethacin-loaded PVP fibres with mean diameters of 2.58±0.3µm for fabrication of wound dressings for transdermal drug delivery [26] whilst Mehta et al used PVP (low and high molecular weight) for coating ocular lenses using both

particles and fibres [27]. PNIPAM polymer engineering using EHDA is scarce. However, PNIPAM hydrogel particles have been yielded using aqueous precipitation polymerization. The particles here ranged between 550nm and 1.60μm; highlighting the potential of the current novel process; a technique useful for the production of smaller particles in a single step with direct deposition control.

Thermal analysis

When using emerging techniques within the pharmaceutical industry, it is imperative to ensure that the processing parameters do not significantly impact the stability of the active or excipients used. DSC was utilised to analyse the thermal transitions of raw materials compared to atomised nano-structures to ensure the solvent (methanol) and the EHDA process has not altered the physical structure of polymers; and subsequently the properties of the resulting nano-architectures. The single, broad points present in the thermograms (**Figure 5a**) for raw materials correspond to each materials melting point. The DSC spectra for the electrically atomised samples also demonstrated similar endothermic peaks to each other with peaks at 115, 113 and 120°C for F1, F2 and F3, respectively. Here, it is noted that the melting point of the atomised formulations are lower than that of the raw drug/materials. This is due to the increased distribution of TM (in the polymeric network) as a result of even molecular dispersion of drug throughout the polymeric matrix during the EHDA process compared to the drug in physical mixture. The thermograms comprise of one peak for each formulation, demonstrating that the original structures of the raw materials was not compromised; highlighting the materials formed polymer-drug complexes and are acting as single system rather than individual components. The resulting DSC scan for F3 particles show a lack of phase characteristic peaks of both PVP and PNIPAM as well as TM, except a broad peak with a maximum of 120°C, (a higher melting point than PVP and PNIPAM alone), suggesting a single, more stable system.

To investigate the thermal behaviour of raw materials and the resultant structures, TGA was conducted. **Figures 5bi** and **5bii** show TGA profiles for raw materials and atomised formulations. The trace for raw TM depicts a sharp weight loss (75.14%) between 201°C and 370°C; shown as a significant decrease between this range. A decline as seen in **Figure 5bi**) is characteristic of drug degradation, as found by Joshi et al [28]. Two major weight loss

events are observed with TGA profiles for both raw polymers. The first weight loss reduction is seen between 40°C and 140°C and between 40°C and 168°C for PVP (11.19% loss) and PNIPAM (3.8% loss) respectively; corresponding to initial moisture loss due to embedded water or residual solvent within the polymer. The second weight loss event is characteristic of polymeric thermal degradation. Within the temperature interval 390°C and 525°, a weight loss of 83.32% can be seen with the PVP TGA trace; where PVP thermally degrades by release of the pyrrolidone side group followed by decomposition on polyenic chains. These results coincide with earlier findings by Peniche et al. [29]. Thermal degradation of PNIPAM can be observed at 342-470°C; a weight loss of 93.18%.

Figure 5bii shows the TGA thermograms of atomised formulations (nano-structures). The profile for all three samples is similar; all three formulations exhibit 2 major weight loss events between 20 and 120°C and between 370 and 485°C. The first weight loss occurrence corresponds to the dispelling of water and the second drastic weight loss is due to matrix polymer degradation. The composite structures degraded at a lower temperature compared to sole polymer-drug samples; which could is a result of polymeric chain arrangement during the EHDA process. The presence of just two weight loss events for nano-structures suggests the polymers and the drug are acting as a single system rather than independent components. As with DSC, the shift at which temperature (or temperature range) product weight loss occurs also indicates drugs encapsulation, which has been previously demonstrated with other actives like indomethacin and naproxen [30].

FTIR

FTIR was performed on raw materials (as obtained powder form) and atomised structures (beaded and particles). The fingerprint of PVP and PNIPAM can be observed using FTIR; as seen in **Figure 6** based on structural groups present. With respect to PVP, peaks at 3469cm^{-1} and 1664cm^{-1} correspond to O-H stretching vibrations and C=O and N-C stretching vibration, respectively. Multiple peaks at 2948cm^{-1}, 2918cm^{-1} and 2875cm^{-1} are present due to CH-CH_2 stretch vibration. Evidence of C-H deformation of cyclic CH_2 groups can be seen at 1492cm^{-1}, 1459cm^{-1}, 1419cm^{-1} and 1371cm^{-1}. Amide III bond (C-N stretching vibration), amide V (CH_2 rocking vibrations) and amide IV bond are present at 1282cm^{-1}, 732cm^{-1} and 648cm^{-1} respectively. Characteristic absorption peaks on the PNIPAM spectra included amide II bond

at 1550cm^{-1}, C=O stretching and CH_3 asymmetric stretching vibrations at 1650cm^{-1} and 2970cm^{-1} ,respectively.

The stability of TM in presence of PVP and PNIPAM (separately and as composite) and following EHDA process can be assessed by analysing the drug-polymer interactions in the resulting spectra from FTIR spectroscopy. A broad band in the spectrum for TM corresponds to O-H/N-H stretching vibrations whilst peaks at 2968cm^{-1}, 2891cm^{-1} and 2854cm^{-1} are present due to aliphatic C-H stretching vibration. The acid carbonyl group of maleic acid and the N-H bending vibrations show peaks at 1707cm^{-1} and 1496cm^{-1}. Bands at 1229cm^{-1} and 954cm^{-1} are due to O-H bending and hydroxyl C-O stretching vibrations, respectively. Similar peaks in the spectra for the atomised formulations indicate the chemical structure of TM was not compromised and was unaffected by the EHDA process.

Contact Angle Analysis

Contact angle (CA) is a quantitative measurement of the wetting of a solid by a liquid (usually water). Angles smaller than 90°C indicate high wettability whilst angles larger than 90°C indicate poor wettability. The wettability of the surface of the electrically atomised samples were characterised and analysed over time **(figure 7).**

Upon dropping the water droplet, the highest static CA was observed with beaded fibers produced by atomising F2 and F3 (130.1°C and 126.27°C, respectively). At t=0 seconds, the CA for TM-loaded PVP particles, an average CA of 83.02°C was recorded (**figure 7d**). This difference in initial CA between particles and fibers could be due to the surface roughness of the structures. The smooth surface of PVP particles (as confirmed through SEM) and high surface area of particles results in less air entrapment between the solid and liquid phases; ultimately resulting in a low static CA as soon as the water droplet comes into contact with the sample [31]. The water droplet applied to F2 samples completely decimated within 10 seconds; indicating rapid penetration of water through the sample, dissolution of sample and/or the increase of degree of wettability with time **(figure 7b).** The CA for F1 and F3 samples were unmeasurable after 10 minutes and 30 minutes respectively due to complete spreading of water after these time points. The polarity of PVP makes the polymer highly hydrophilic; indicating a low CA at t=0 seconds. However, the density of the samples can cause particles to agglomerate, trapping air between the particles. This may prevent the

water droplet penetrating and spreading. The dissolution of PVP over time allows the water penetrate the inter-particle pores and spread; with the droplet spreading completely within 10 minutes of application [32]. The combination of particles and fibers with F3 samples increases the surface area and surface roughness of the sample; which in turn can contribute to the time it took for the CA to reduce from an average of 126°C at t=0 seconds to 0°C at t=1800 seconds.

In vitro timolol release

Evaluation of TM release from the atomised structures was carried using *in vitro* method. **Figure 8** shows percentage cumulative release of TM from polymeric nano-structures in PBS at physiological conditions (pH=7.4, 37°C). The release study shows at t=1 minute; 25, 12.4 and 11% TM was released from F1, F2 and F3 atomised formulations, respectively. At t= 30 mins, over 50% of TM was released from all three atomised samples. At t = 24 hours, drug release was found to be 89.8% for F2, whereas for F1 and F3 formulations, only 63.2 and 68.2% of TM was released, respectively. There is a noticeable general trend for all three formulations; similar release profiles can be observed. There is an initial burst release, followed by sustained, controlled release over time, eventually plateauing at *t* = 24 hours.

The rapidly dissolving nature of PVP explains the initial rapid release seen with F1 and F3. Coatings with beaded morphology (i.e. F2 and F3) account for the initial rapid release observed as nano-structures tend to release drug more quickly due to higher surface area. PVP has been used often in ophthalmic formulations such as a rapidly dissolving matrix for the delivery of rifampicin[33] and in the manufacture of ocular films for delivery of anti-inflammatory drug diclofenac sodium[34] which displayed controlled drug release showing more than 50% of drug to be released within 1 hour and the remaining drug released within 4 hours[34]. Controlled release of drug using PNIPAM has been previously shown where the polymer has been used as a nano-vesicular carrier for anticancer drug 5-fluorouracil [35]. Furthermore, an increase in physiological temperature exhibited sustained drug release with 35% of drug released within 24 hours. The combination of a fast dissolving polymer (PVP) and a more sustained dissolving polymer (PNIPAM) along with the emerging EHDA can be used to develop polymeric device coatings with controlled and prolonged release, as shown by these *in vitro* studies.

Probe release

To demonstrate drug leaving the polymer matrix at a sustained rate as well as the polymer remaining on the device, lenses were coated with atomised probe-loaded polymeric nano-structures and exposed to PBS in similar fashion to *in vitro* TM release. **Figure 9** displays the release profile of Rhodamine from the lens into PBS by showing both DI on the lens visually (fluorescence images) and DI in PBS, using UV-Spectroscopy. For PVP coated lenses, there is 100% DI on lens at t=0mins and 0 DI in PBS. As time increases, DI on lens decreases (down to 8.7%) (**Figure 9a**) and the DI in PBS increases (up to 0.034). An initial burst release between t=0mins and t=10mins (100% to 43% DI on lens) was exhibited which gradually plateaued after t=6 hours (9.79% DI on lens). Data collated from UV spectroscopy supported data using fluorescence microscopy; initial burst release of probe into PBS from 0 to 0.0064 within the first 10 mins of exposure which then gradually increased to 0.034 after 24 hrs. For PNIPAM coated lens, a similar release profile was observed as with PVP; initial burst release followed by sustained release. **Figure 9bi** shows fluorescence images of each contact lens after removal from PBS and **Figure 9bii** shows the release profiles of Rhodamine B from the lens and into PBS. DI on the lens decreases rapidly within 10 minutes (65.5% of probe was released) and the profile of release into PBS shows a sudden initial increase (from 0 to 0.01) within 10 minutes with subsequent gradual increase after 1 hour (0.016) to 24 hrs (0.047). With respect to the composite coated lenses an initial burst release with subsequent sustained release was observed with approximately 50% of the probe being released into the media and 50% remaining on the lens (**Figure 9cii**). After 6 hours, 71% of the dye had been released from the polymeric coatings and following the 24 hr mark, 89% of the probe had been released into PBS. The sustained release of Rhodamine B was exhibited from 10 mins (0.07667; absorbance in PBS) to 24 hours (0.0426).

Release kinetics

To determine which type of release mechanism was prominent in this study, data from *in vitro* release of TM was fitted to various kinetic models to obtain graphical plots. The linearity of graphs was demonstrated by the regression co-efficient, R^2 (**Table 2**); the higher the R^2 value, the more linear the graph, the better the correlation between the variables. Drug release following zero-order kinetics demonstrates a release independent to the drug

concentration whilst first-order kinetics indicate the release of drug is concentration dependent (**Table 2)**

In order to determine if the release of TM was zero order, the cumulative percentage release of TM was plotted against time. For analysis of first order kinetics, log cumulative percentage of TM release was plotted as a function of time.

Hixson-Cromwell cube root law is describes the release of drug due to change in particle surface area and diameter[36], where the cube root of percentage of drug remaining in the matrix is plotted versus time.

The Higuchi model describes drug dissolution from various types of modified release from polymeric matrices. The model was originally intended for planar systems but evolved to extend to different geometries and porous matrices. The Higuchi model has been generalised to yield the simplified Higuchi Model [37].

The Higuchi model is based on several hypotheses; i) initial drug concentration in the matrix is much higher than drug solubility; ii) drug diffusion is only in one plane; iii) drug particles are much smaller than the system matrix; iv) the matrix swelling and dissolution is negligible; v) drug diffusivity is constant; vi) perfect sink conditions in release environment are reached. The cumulative drug release of TM from all three samples was plotted as function of square root of time.

The Korsmeyer-Peppas model was devised to explain the type of diffusive mechanism from polymeric matrix. **Equation 3** shows the Korsmeyer-Peppas model;

$$\frac{M_t}{M_\infty} = k\, t^n \qquad \textbf{(Eqn.3)}$$

Where M_t/M_∞ is the proportion of drug released at time, t; k is the release rate constant and n is the release exponent; the factor that determines the mechanism of drug release. **Equation 4** shows how to derive the release exponent.

$$\log\left(\frac{M_t}{M_\infty} \times 100\right) = n \log t \times \log k \qquad \textbf{(Eqn. 4)}$$

The Korsmeyer-Peppas model is pragmatic when there are multiple possible release mechanisms. For spherical matrices, various n values depict specific release mechanisms; $n \leq 0.45$ corresponds to quasi-Fickian drug transport, n=0.5 shows Fickian diffusion (molecular diffusion of drug due to a chemical potential gradient) , $0.45<n<0.89$ relates a Non- Fickian diffusion mechanism, n=0.89 relates to the case II transport with $n>0.89$ corresponds to the super case II transport[38] (drug transport mechanism associated with stresses and state transition in hydrophilic glassy polymers which swell in water and other biological fluids)[39]. Log cumulative release (%) was plotted as a function of log t; here only the first 60% was fitted to the Korsmeyer-Peppas model with resulting parameters collated from the model given in **Table 3**.

All three formulations showed a poor fit for zero order and first order release kinetics, confirmed by low r^2 values **(Table 2)**. Results from the Hixson Cromwell model indicate the release of TM was not limited by dissolution but by the transport of drug through the polymeric matrix. Adequate linearity across all 3 TM loaded polymeric samples (F1, F2 and F3) were observed with the Higuchi Model (**Table 2**); suggesting TM release is a diffusive mechanism, in particular it is likely to be quasi-Fickian Diffusion. This is mirrored in the coefficient of determination (R^2) of 0.5073, 0.6227 and 0.5021 for F1, F2 and F3 atomised formulations, respectively. Data collated from the Korsmeyer-Peppas model is shown in **Table 3**. For F1, F2 and F3, the n values were 0.1588, 0.1964 and 0.4921, respectively, which also indicate quasi-Fickian transport dominated the release of TM in PBS from polymeric nano-structures. Therefore the release mechanism of TM here was diffusion dominated [38,39].

Biological Evaluation of TM-Loaded Nanoparticles

The BCOP test is an organotypic assay utilised to assess the irritancy of test materials based on how corneal opacity and permeability is affected. An undamaged cornea is a clear structure which acts as a protective barrier which enables the cornea to remain impermeable to a large array of materials including sodium fluorescein dye. Hence, any damage to the cornea following treatment with test substances can be associated with said substances.

Figures 10a-c illustrates the response of bovine cornea opacity to TM-loaded nano-structures alongside controls. Visual observation of the cornea confirms normal saline, the concurrent negative control, shows no damage to the cornea. There is also no change in the opacity of the cornea. In contrast, for the positive control, NaOH, unmistakable opacification can be detected; indicating the most severe damage to the cornea. Application of NaOH to the cornea results in interactions with corneal cell membranes. Subsequently, fatty acids in these cells undergo saponification; compromising not only the tight junctions between the corneal epithelial cells but the whole epithelium layer [40]; increasing the permeability of the cornea to the fluorescein dye. Clear visual evidence under a cobalt blue filter (465-490nm) indicates that the fluorescein dye has permeated through the corneal layers in NaOH-treated cornea as seen in **Figure 10h**). The mild positive control (acetone) exhibited a faint cloudy region, suggesting acetone to be a mild irritant to the eye. Acetone causes partial injury to epithelial cells as a result of lipid solvent interaction properties which can irritate mucosal membranes; ultimately resulting in eye irritation; demonstrated under a cobalt light filter as slight fluorescence (**Figure 10i**). The bovine cornea treated with normal saline exhibited no fluorescence, showing the dye had not permeated the cornea; highlighting the integrity of the cornea was not compromised. Similar results were yielded from TM-loaded ocular lenses; showing F1, F2 and F3 did not damage the cornea and are therefore biocompatible formulations for ocular device coating (**Figures 10j-l).**

Ex vivo corneal permeation of TM

Ex vivo permeation studies can provide an insight to how the electrically atomised formulations release drug and how the active permeates or penetrates the targeting tissue. TM permeation from atomised nano-structures was measured using freshly excised bovine corneas **(figure 1e).** Various parameters (steady state flux (J_{ss}), apparent permeation coefficient (P_{app})) were derived from this *ex vivo* study. **Figure 11** shows the ex vivo permeation of TM over time whilst **Table 4** shows the steady state flux and P_{app} values for all three atomised formulations. Statistical analysis (one way ANOVA) was conducted to report the statistical significance between the three formulations. The results showed a significant difference in ex vivo permeation between all three formulations ($F(3,28)=3.340$, $p=0.033$) with regards to the amount of TM permeating through the excised cornea. The permeation rate of TM from F3 formulation was the highest (J_{ss}=4.431µg.cm^{-2}.h^{-1}; P_{app} = 0.9334cm.h^{-1})

and was the lowest F1 (J_{ss}=0.86977 µg/cm^2/h; P_{app} = 0.2827cm/h^{-1}). This difference is due to the combination of rapidly dissolving polymer (PVP) and thermosensitive, slowly dissolving polymer (PNIPAM) allowing the facilitation of TM corneal drug delivery. Based on a study by Moosa the *in vivo* effect on TM release from ocular inserts, marketing eye drops demonstrated P_{app} of 1.7x10^{-4} cm.min^{-1} and J_{ss} = 0.00052 mg.cm^{-2}.min^{-1} in rabbit eyes. The values are contrastingly higher that those derived in this study suggesting atomised (coated) lenses could lead to a reduction in frequent dosing and medicated applications. This reduction, in turn, has potential to minimise risk of ocular toxicity as a result of lowered systemic drug absorption [41]. Furthermore, such systems provide greater potential for patient compliance.

Conclusion

A variety of fibrous polymeric matrices incorporating TM were developed as on demand ocular lens coatings exhibiting sustained release of the glaucoma drug. Detailed analysis confirmed the viability of lens coatings. The novelty of combining an on demand EHDA engineering process for drug delivery *via* stabilised contact lens formulation has not yet been explored in great depth, and the current work demonstrates exciting possibilities.

References

[1] World Health Organisation (WHO), http://www.who.int/blindness/causes/priority/en/index6.html 01/05/2015 (2015).

[2] J. Morrison, I. Pollack, Glaucoma: Science and Practice, 1st ed., Thieme Medical Publishers, Hong Kong, 2002.

[3] C. Peng, M.T. Burke, B.E. Carbia, C. Plummer, A. Chauhan, Extended drug delivery by contact lenses for glaucoma therapy, J. Control. Release 162 (2012) 152-158.

[4] I.M. Carvalho, C.S. Marques, R.S. Oliveria, P.B. Coelho, P.C. Costa, D.C. Ferreira, Sustained Drug Release by contact lenses for Glaucoma Treatment - a review, J. Control. Release 202 (2015) 76-82.

[5] U.B. Kompella, R.S. Kadam, V.H.L. Lee, Recent Advances in ophthalmic drug delivery., Ther. Deliv. 3 (2010) 435-456.

[6] V.R. Kearns, R.L. Williams, Drug Delivery Systems for the eye., Expert Rev. Med. Devices 6 (2009) 277-290.

[7] A. ElShaer, B. Ghatora, S. Mustafa, R.G. Alany, Contact lenses as drug reservoirs & delivery systems: the successes & challenges., Ther. Deliv. 5 (2014) 1085-1100.

[8] J. Wheeler, J. Woods, M. Cox, R. Cantrell, F. Watkins, R. Edlich, Evolution of hydrogel polymers as contact lenses, surface coatings, dressings, and drug delivery systems, J. Long. Term. Eff. Med. 6 (1996) 207-217.

[9] A. Hui, H. Sheardown, L. Jones, Acetic and Acrylic Acid Molecular Imprinted Model Silicone Hydrogel Materials for Ciprofloxacin-HCl Delivery, Materials. 5 (2012) 85-107.

[10] P. Andrade-Vivero, E. Fernandez-Gabriel, C. Alvarez-Lorenzo, A. Concheiro, Improving the loading and release of NSAIDs from pHEMA hydrogels by copolymerization with functionalized monomers, J. Pharm. Sci. 96 (2007) 802-813.

[11] G. Hollo, A. Katsanos, Safety and tolerability of the tafluprost/timolol fixed combination for the treatment of glaucoma., Exp. Opin. Drug Saf. 14 (2015) 609-17.

[12] L.C. Bengani, A. Chauhan, Extended delivery of an anionic drug by contact lens loaded with a cationic surfactant, Biomaterials. 34 (2013) 2814-2821.

[13] C. Peng, J. Kim, A. Chauhan, Extended delivery of hydrophilic drugs from silicone-hydrogel contact lenses containing Vitamin E diffusion barriers, Biomaterials. 31 (2010) 4032-4047.

[14] H.J. Jung, M. Abou-Jaoude, B.E. Carbia, C. Plummer, A. Chauhan, Glaucoma therapy by extended release of timolol from nanoparticle loaded silicone-hydrogel contact lenses, J. Control. Release 165 (2013) 82-89.

[15] G. Guidi, M. Korogiannaki, H. Sheardown, Modification of timolol release from silicone hydrogel model contact lens materials using hyaluronic acid, Eye.Contact. Lens 40 (2014) 269-276.

[16] P. Paradiso, R. Galante, L. Santos, A.P. Alves de Matos, R. Colaco, A.P. Serro, B. Saramago, Comparison of two hydrogel formulations for drug release in ophthalmic lenses, J. Biomed. Mat. Res. Part B. App. Biomatt. 102 (2014) 1170-1180.

[17] S. Mohammadi, L. Jones, M. Gorbet, Extended Latanoprost Release from Commercial Contact Lenses: In Vitro Studies Using Corneal Models, PLoS One 9 (2014) e106653.

[18] A. Hui, M. Willcox, L. Jones, In Vitro and In Vivo Evaluation of Novel Ciprofloxacin-Releasing Silicone Hydrogel Contact Lenses, Invest. Ophthalmol. Vis. Sci. 55 (2014) 4896-4904.

[19] C. Lu, R.B. Yoganathan, M. Kociolek, C. Allen, Hydrogel containing silica shell cross-linked micelles for ocular drug delivery, J. Pharm. Sci. 102 (2013) 627-637.

[20] P. Mehta, R. Haj-Ahmad, M. Rasekh, M.S. Arshad, A. Smith, S.M. van der Merwe, X. Li, M. Chang, Z. Ahmad, Pharmaceutical and biomaterial engineering via electrohydrodynamic atomization technologies, Drug Discov. Today (2017).

[21] Y. Lee, B. Wu, W. Zhuang, D. Chen, Y.J. Tang, Nanoparticles facilitate gene delivery to microorganisms via an electrospray process, J. Microbiol. Methods 84 (2011) 228-233.

[22] M. Zamani, M.P. Prabhakaran, E.S. Thian, S. Ramakrishna, Protein encapsulated core-shell structured particles prepared by coaxial electrospraying: Investigation on material and processing variables, Int. J. Pharm. 473 (2014) 134-143.

[23] L.H. Lima, Y. Morales, T. Cabral, Ocular Biocompatibility of Poly-N-Isopropylacrylamide (pNIPAM), J. Ophthalmol. (2016) 5356371.

[24] A. Jaworek, A. Krupa, Classification of the modes of EHD spraying, J. Aerosol Sci. 30 (1999) 873-893.

[25] R.R. Haj-Ahmad, A.A. Elkordy, C.S. Chaw, A. Moore, Compare and contrast the effects of surfactants (Pluronic®F-127 and Cremophor®EL) and sugars (β-cyclodextrin and inulin) on properties of spray dried and crystallised lysozyme, Eur. J. Pharm. Sci. 49 (2013) 519-534.

[26] M. Rasekh, C. Karavasili, Y.L. Soong, N. Bouropoulos, M. Morris, D. Armitage, X. Li, D.G. Fatouros, Z. Ahmad, Electrospun PVP-indomethacin constituents for transdermal dressings and drug delivery devices, Int. J. Pharm. 473 (2014) 95-104.

[27] P. Mehta, L. Justo, S. Walsh, M.S. Arshad, C.G. Wilson, C.K. O'Sullivan, S.M. Moghimi, I.S. Vizirianakis, K. Avgoustakis, D.G. Fatouros, Z. Ahmad, New platforms for multi-functional ocular lenses: engineering double-sided functionalized nano-coatings, J. Drug Target. 23 (2015) 305-310.

[28] G.V. Joshi, B.D. Kevadiya, H.A. Patel, H.C. Bajaj, R.V. Jasra, Montmorillonite as a drug delivery system: Intercalation and in vitro release of timolol maleate, Int. J. Pharm. 374 (2009) 53-57.

[29] C. Peniche, D. Zaldívar, M. Pazos, S. Páz, A. Bulay, J.S. Román, Study of the thermal degradation of poly(N-vinyl-2-pyrrolidone) by thermogravimetry-FTIR, J Appl Polym Sci 50 (1993) 485-493.

[30] P. Taepaiboon, U. Rungsardthong, P. Supaphol, Drug-loaded electrospun mats of poly(vinyl alcohol) fibres and their release characteristics of four model drugs, Nanotechnology 17 (2006) 2317-2329.

[31] W. Ma, Z. Guo, J. Zhao, Q. Yu, F. Wang, J. Han, H. Pan, J. Yao, Q. Zhang, S.K. Samal, S.C. De Smedt, C. Huang, Polyimide/cellulose acetate core/shell electrospun fibrous membranes for oil-water separation, Sep. Purif. Technol. 177 (2017) 71-85.

[32] J. Kim, E. Kim, S.S. Kim, Micro-nano hierarchical superhydrophobic electrospray-synthesized silica layers, J. Colloid. Interface. Sci. 392 (2013) 376-381.

[33] S. Braha, C. Gafitanu, E. Braha, C. Tuchilus, M. Vasilescu, A. Poiata, Enhancement of Dissolution of Rifampicine and in Vitro/in Vivo Evaluation of Drug Release from Collyrium, Farmacia 57 (2009) 58-64.

[34] Z. Jafariazar, N. Jamalinia, F. Ghorbani-Bidkorbeh, S.A. Mortazavi, Design and Evaluation of Ocular Controlled Delivery System for Diclofenac Sodium, Iran. J. Pharm. Res. 14 (2015) 23-31.

[35] G. Li, M. Qi, N. Yu, Q. Tao, Polymer vesicles assembled from ALG-g-PNIPAM and β-cyclodextrin through inclusion complexation for drug release, J. Control. Release 213 (2015) e35.

[36] A.W. Hixson, J.H. Cromwell, Dependence of Reaction Velocity upon Surface Agitation, Ind, Eng, Chem. 23 (1931) 923-931.

[37] J. Siepmann, N.A. Peppas, Higuchi Equation: Derivation, applications, use and misuse., Int. J. Pharm. 418 (2011) 6-12.

[38] P.L. Riger, N.A. Peppas, A siuple equation for description of solute release: II. Fickian and anomalous release from swellable devices., J. Control. Release (1987) 37-42.

[39] R.W. Korsmeyer, R. Gurny, E. Doelker, P. Buri, N.A. Peppas, Mechanisms of solute release from porous hydrophilic polymers., Int. J. Pharm. 15 (1983) 25-35.

[40] M. Reim, N.F. Schrage, J. Becker, Interactions between ocular surface fluid and cornea related to contact lenses, Eur. J. Ophthalmol. 11 (2001) 105-115.

[41] R.M. Moosa, Y.E. Choonara, P. Kumar, L.C. du Toit, L.K. Tomar, C. Tyagi, T.R. Carmichael, V. Pillay, In vivo evaluation and in-depth pharmaceutical characterization of a rapidly dissolving solid ocular matrix for the topical delivery of timolol maleate in the rabbit eye model, Int. J. Pharm. 466 (2014) 296-306.

Tables and Figures Captions

Tables

Table1. Formulated sample composition and their loading efficiency. Polymer concentrations were 5% w/v and timolol maleate concentration 5% w/w of the polymer. [PVP: polyvinylpyrrolidone, PNIPAM: poly (N-isopropylacrylamide), TM: timolol maleate]

Table 2. Kinetic models for timolol maleate release expressed by regression coefficient, R^2. * Where C_t is the amount of drug released at time *t*, C_0 is the initial amount of drug in release medium and k_0 is the zero-order rate constant. ** Where C_0 is the initial concentration of drug in the formulation, C indicates unreleased drug in formulation and K is the first order release constant. *** Where M_t is the quantity of cumulative drug released at time t, and k_H is the Higuchi constant.

Table 3. Korsmeyer-Peppas model parameters for timolol maleate release

Table 4. Summary of parameters derived from *ex-vivo* release studies

Figures

Figure 1. (a) EHDA set-up (b) and (c) close-up lens substrate (d) diagrammatic presentation (e) Preparation of bovine cornea for ex-vivo drug release

Figure 2. Flow of liquid under an electrical field using a single conductive needle under a) no flow, b) dripping mode. Stable cone jet formation when spraying c) F1, d) F2 and e) F3 Jetting mode-map profiles for f) F1, g) F2 and h) F3

Figure 3. a) Digital images of an uncoated lens, b) thin coated lens, c) densely coated lens, optical micrographs showing electrically atomised coatings of d) F1, e) F2 and f) F3. Electron micrographs of coatings at 5k magnification g) F1, h) F2 and i) F3 respectively and at 50k magnification j) F1, k) F2 and l) F3 respectively. Probe encapsulation m) fluorescence of PVP-Rhodamine B, n) fluorescence of Rhodamine B-loaded PNIPAM nano-structures and o) Rhodamine B- composite polymer

Figure 4. Particle size distribution of polymeric particles

Figure 5. Thermal analysis of atomised coatings a) DSC thermograms of raw materials and atomised samples. b) TGA thermograms for i) raw materials and ii) electrically atomised samples.

Figure 6. FTIR spectra for raw materials and atomised structures.

Figure 7. Contact angle analysis. Digital images taken during contact angle measurements over time for a) F1 samples, b) F2 samples, c) F3 samples at i) 0 seconds, ii) 30 seconds, iii) 10 minutes and iv) 30 minutes, d) Contact Angle analysis over time for F1, F2 and F3.

Figure 8. *In vitro* cumulative drug release (%) from various polymeric nano-structures.

Figure 9. a) PVP i) fluorescence images of dye-loaded F1 NPs coating on lenses. ii) Profile of dye* Intensity on lens at various time increments and dye* Intensity in PBS as a function of time , b) PNIPAM i) fluorescence images of dye-loaded F2 NPs coating on lens, ii) profile of dye* intensity of lens (vs. time increments) and dye* intensity in PBS as function of time.

Figure 10. BCOP results of freshly excised bovine cornea. Digital images of treated cornea: a) negative control, b) positive control, c) slightly positive control, d) F1, e) F2 and f) F3 and fluorescence images under cobalt blue filter g) negative control, h) positive control, i) slightly positive control, j) F1, k) F2 and l) F3

Figure 11. Ex vivo cumulative drug amount (µg) permeated across excised bovine cornea.

Tables

Table 1

Formulation	Composition	Loading Efficiency (%)
F1	PVP , TM	64.63
F2	PNIPAM, TM	79.8
F3	PVP, PNIPAM, TM	99.7

Table 2

Formulation	Zero-order	First-order	Hixson-Cromwell	Higuchi
	$* C_t = C_0 + k_0 t$	$** \log C = \log C_0 - Kt/2.303$	$W_0^{\frac{1}{3}} - W_t^{\frac{1}{3}} = kt$	$*** Mt = k_H\sqrt{t}$
F1	0.1826	0.2092	0.0596	0.5073
F2	0.3376	0.2217	0.1377	0.6227
F3	0.2355	0.1604	0.0912	0.5021

Table 3

Formulation	R^2	n
F1	0.8107	0.1588
F2	0.7967	0.4921
F3	0.6932	0.1964

Table 4

	F1	F2	F3
Sample Weight (mg)	1.33±0.058	4.10±0.70	1.63±0.58
% Permeated / Surface area (%/cm²) after 24 hours	60.13±5.51	47.70±5.07	90.11±8.95
Steady State Flux (µg/cm²/min)	0.017±0.0038	0.020±0.00081	0.057±0.017
Apparent Permeability Coefficient (cm²/min)	0.0055±0.0012	0.0052±0.00021	0.012±0.0038

*Values presented are mean± standard deviation

Figures

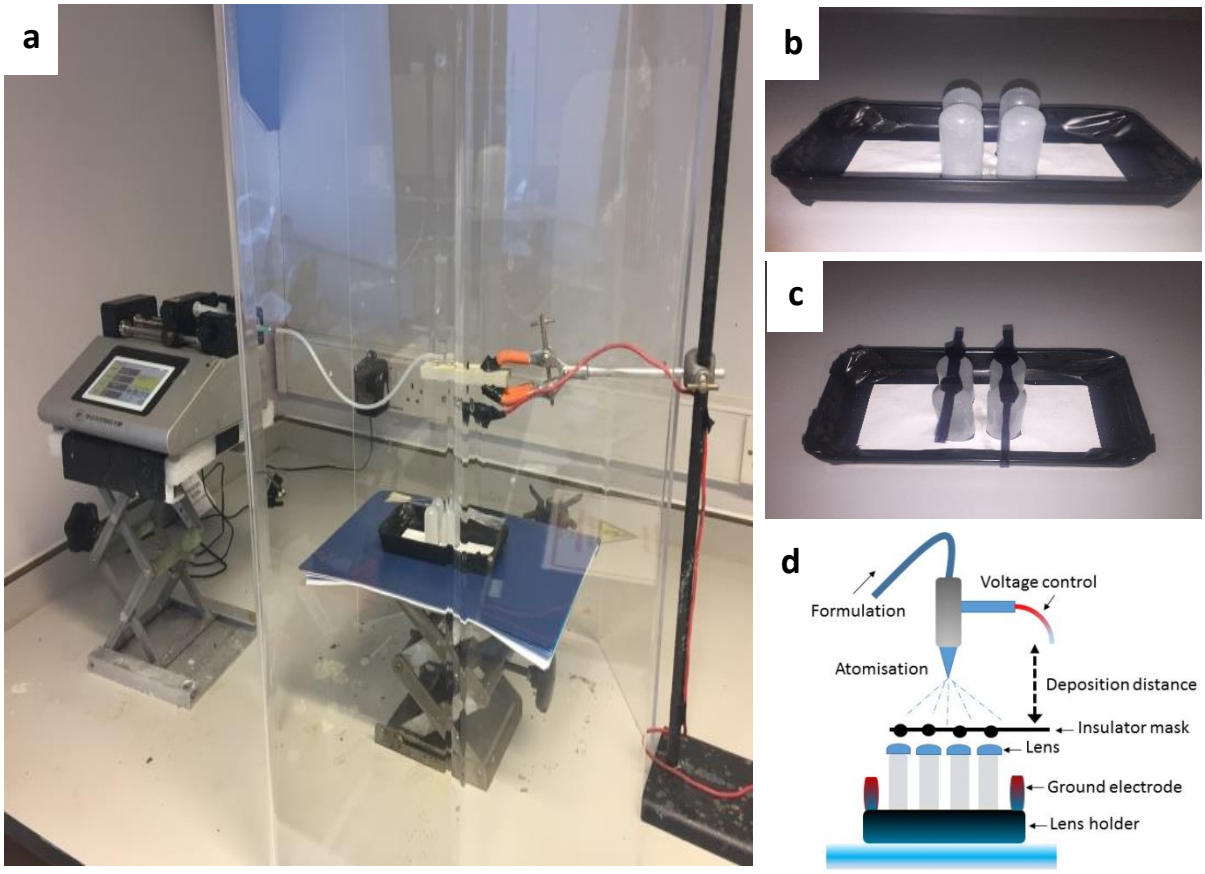

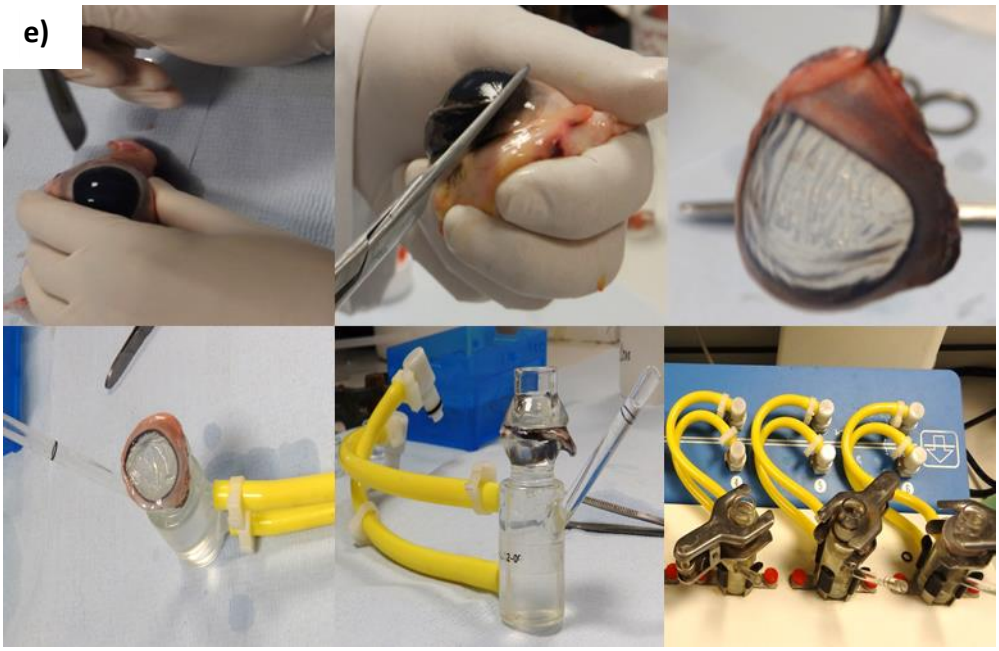

Figure 1

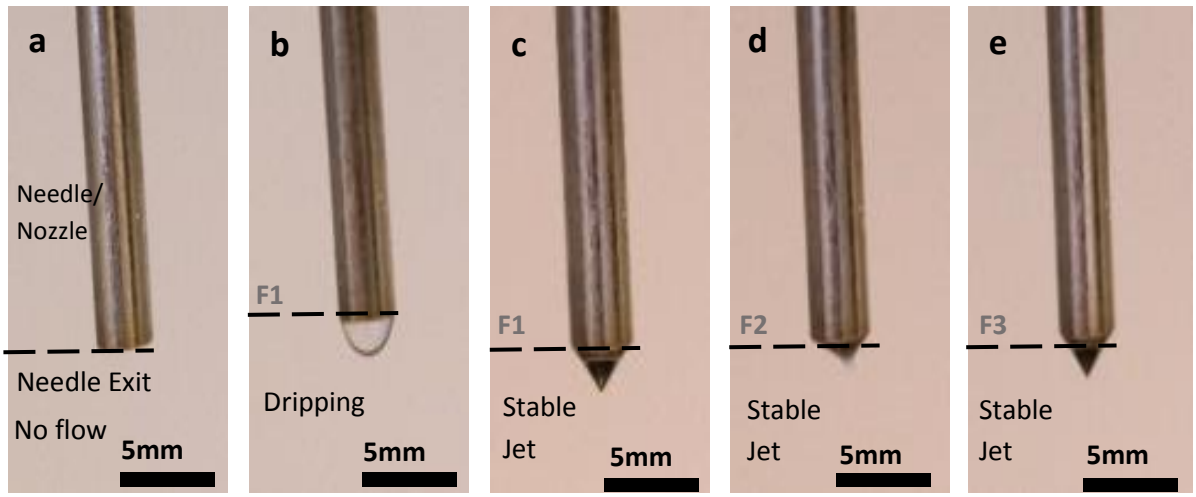
a
Needle/
Nozzle
Needle Exit
No flow
5mm
b
F1
Dripping
5mm
c
F1
Stable
Jet
5mm
d
F2
Stable
Jet
5mm
e
F3
Stable
Jet
5mm

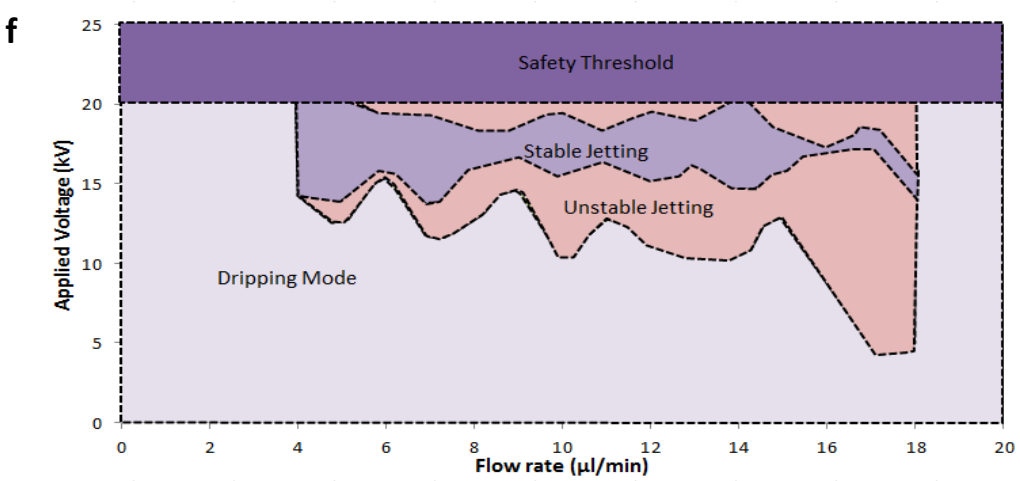
f
Safety Threshold
Stable Jetting
Unstable Jetting
Dripping Mode
Applied Voltage (kV)
Flow rate (µl/min)

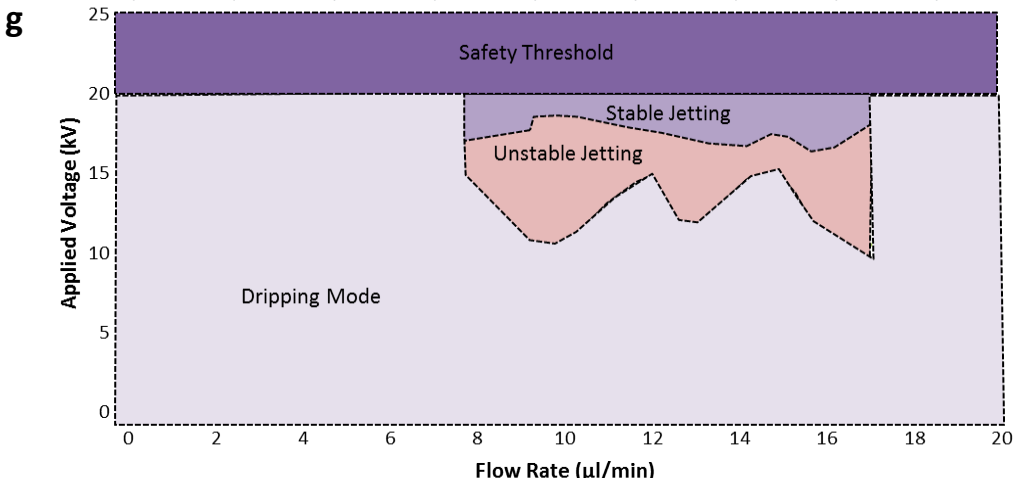
g
Safety Threshold
Stable Jetting
Unstable Jetting
Dripping Mode
Applied Voltage (kV)
Flow Rate (ul/min)

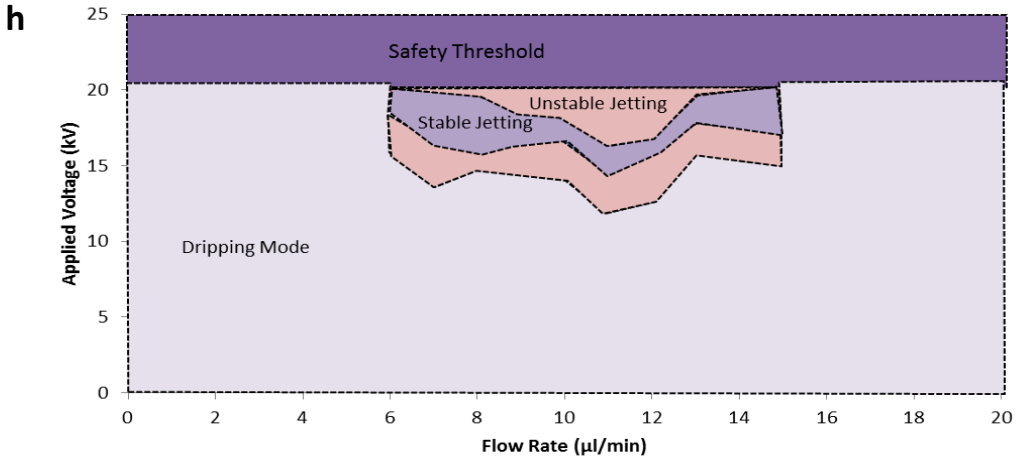
h
Safety Threshold
Unstable Jetting
Stable Jetting
Dripping Mode
Applied Voltage (kV)
Flow Rate (µl/min)

Figure 2

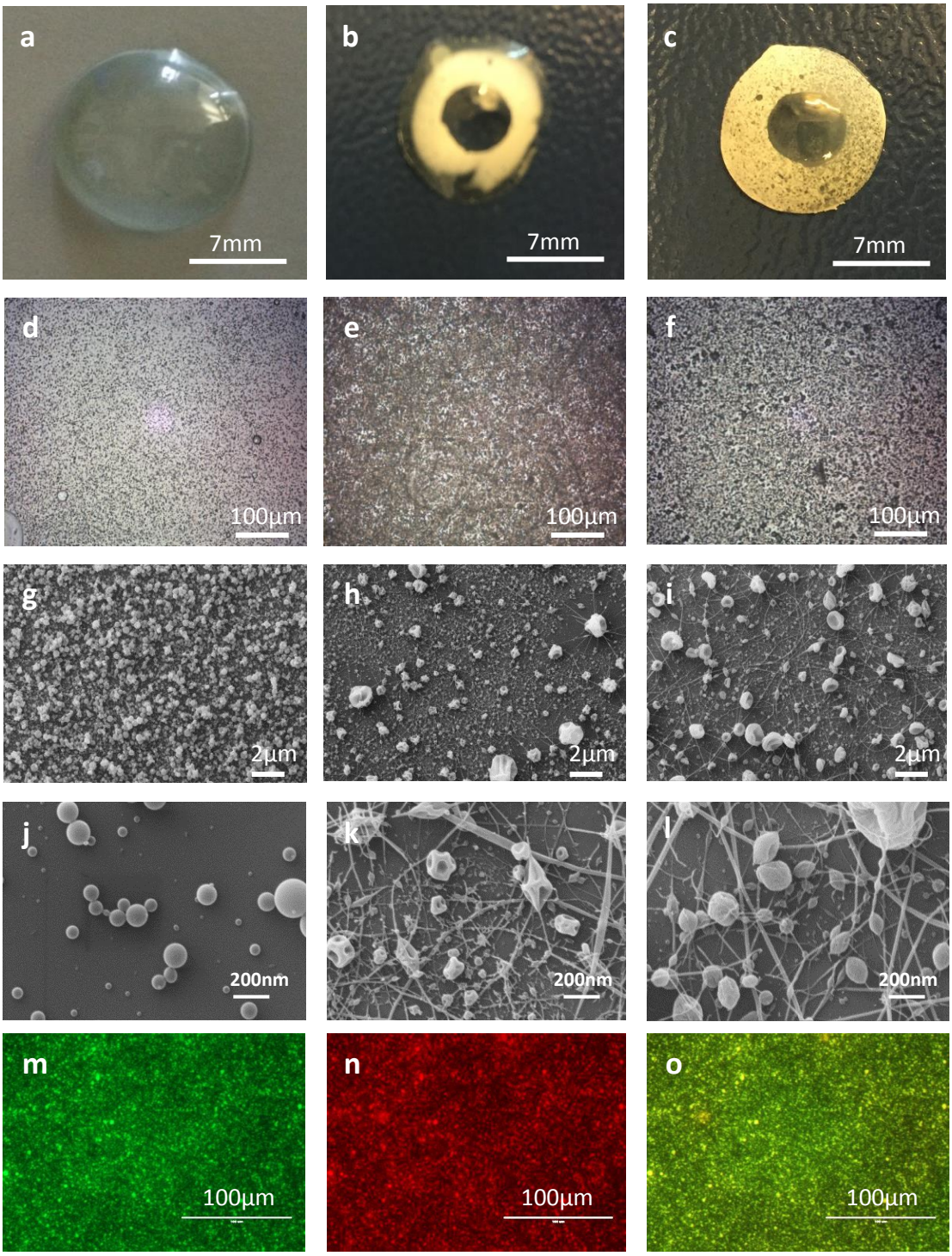
a
7mm
b
7mm
c
7mm
d
100µm
e
100µm
f
100µm
g
2µm
h
2µm
i
2µm
j
200nm
k
200nm
l
200nm
m
100µm
n
100µm
o
100µm

Figure 3

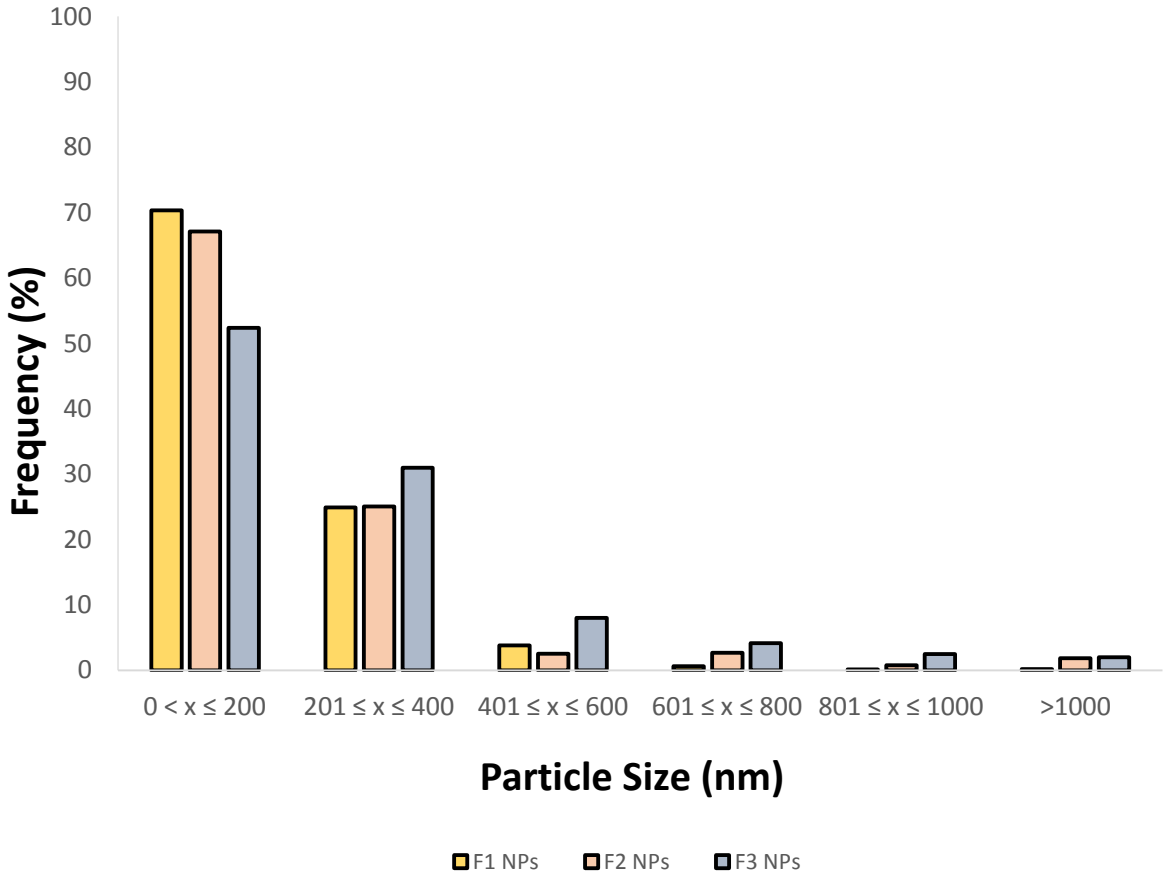
100
90
80
70
60
50
40
30
20
10
0
Frequency (%)
0 < x ≤ 200
201 ≤ x ≤ 400
401 ≤ x ≤ 600
601 ≤ x ≤ 800
801 ≤ x ≤ 1000
>1000
Particle Size (nm)
F1 NPs
F2 NPs
F3 NPs

Figure 4

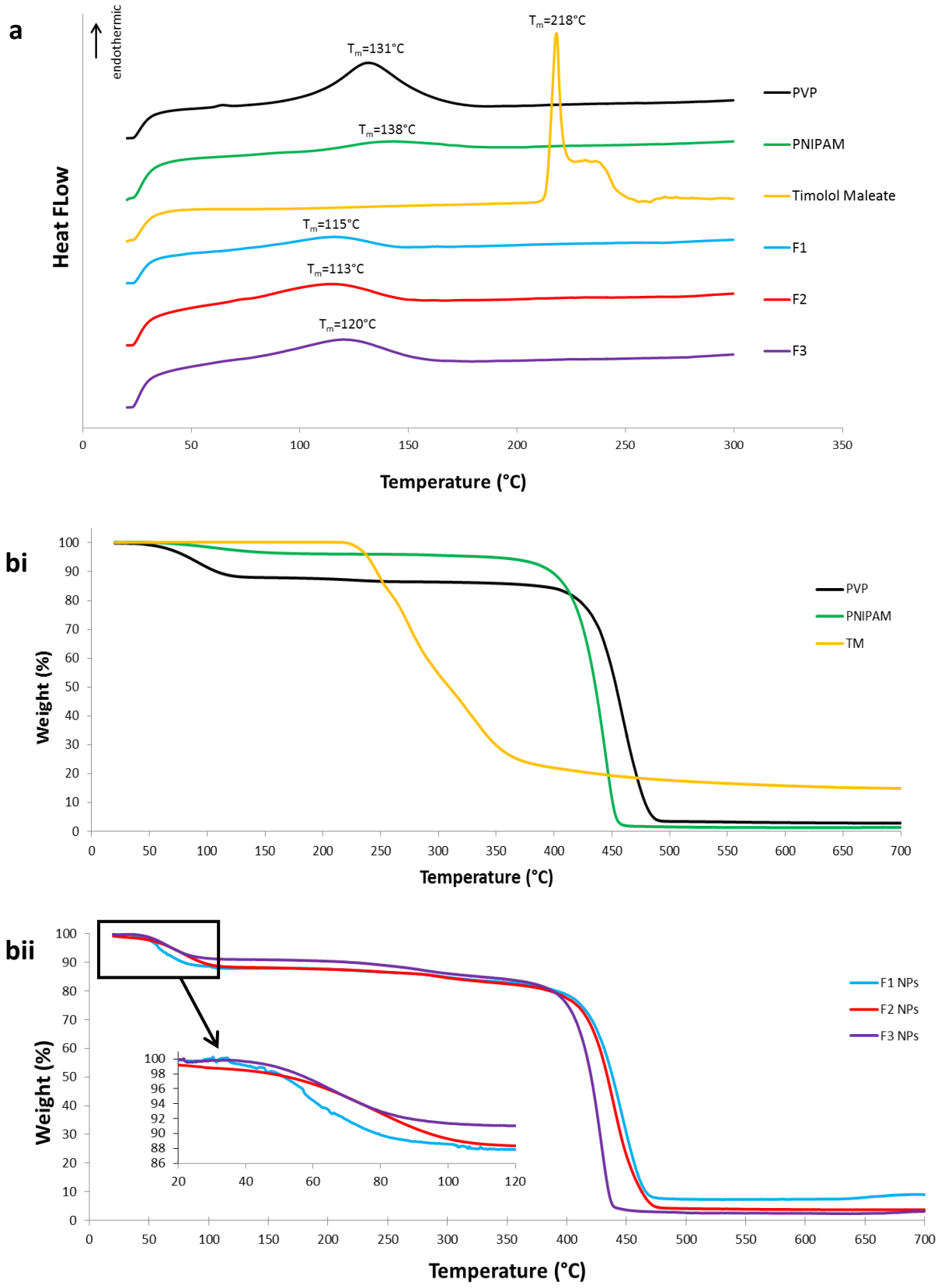
a
endothermic
Heat FLow
Tm=131°C
Tm=218°C
Tm=138°C
Tm=115°C
Tm=113°C
Tm=120°C
PVP
PNIPAM
Timolol Maleate
F1
F2
F3
Temperature (°C)
bi
Weight (%)
PVP
PNIPAM
TM
Temperature (°C)
bii
Weight (%)
F1 NPs
F2 NPs
F3 NPs
Temperature (°C)

Figure 5

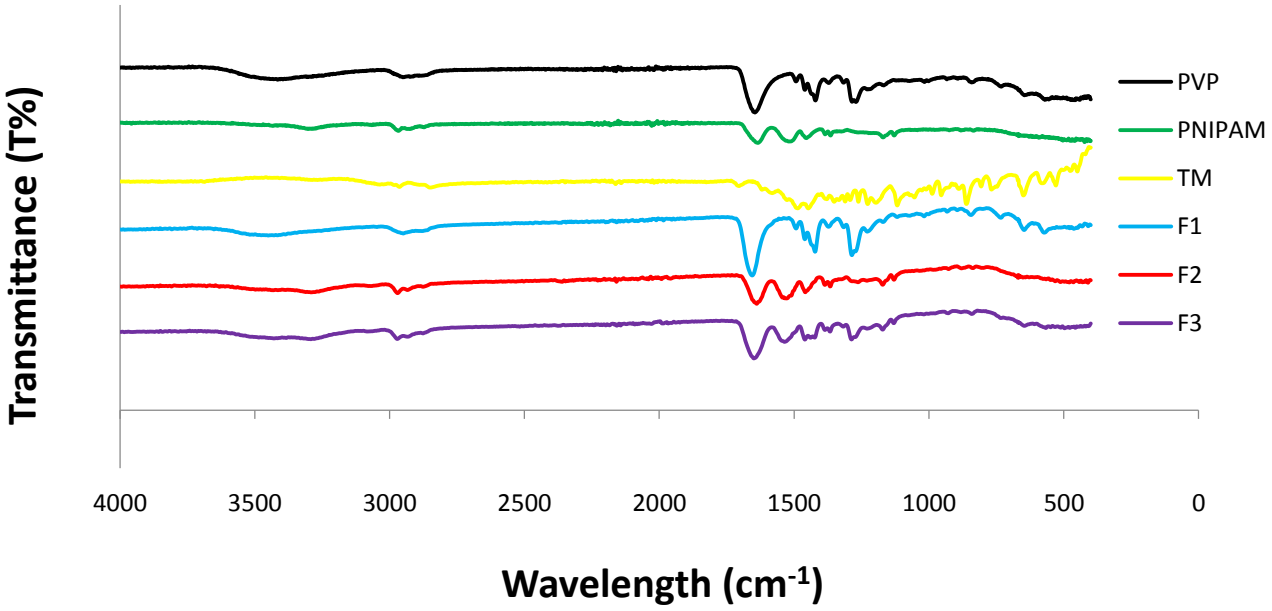
Transmittance (T%)
PVP
PNIPAM
TM
F1
F2
F3
4000
3500
3000
2500
2000
1500
1000
500
0
Wavelength (cm-1)

Figure 6

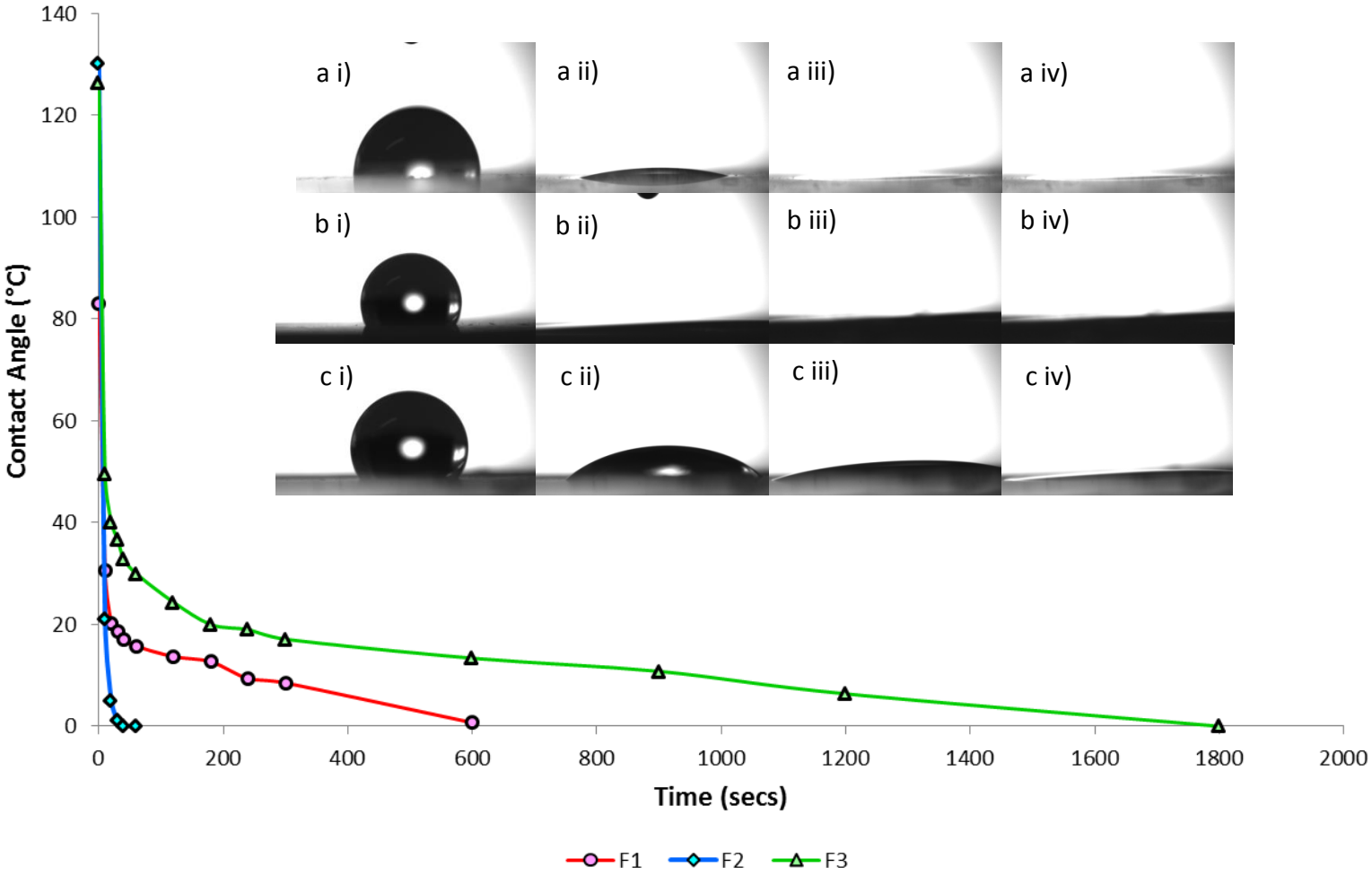
a i)
a ii)
a iii)
a iv)
b i)
b ii)
b iii)
b iv)
c i)
c ii)
c iii)
c iv)
Contact Angle (°C)
Time (secs)
F1
F2
F3

Figure 7

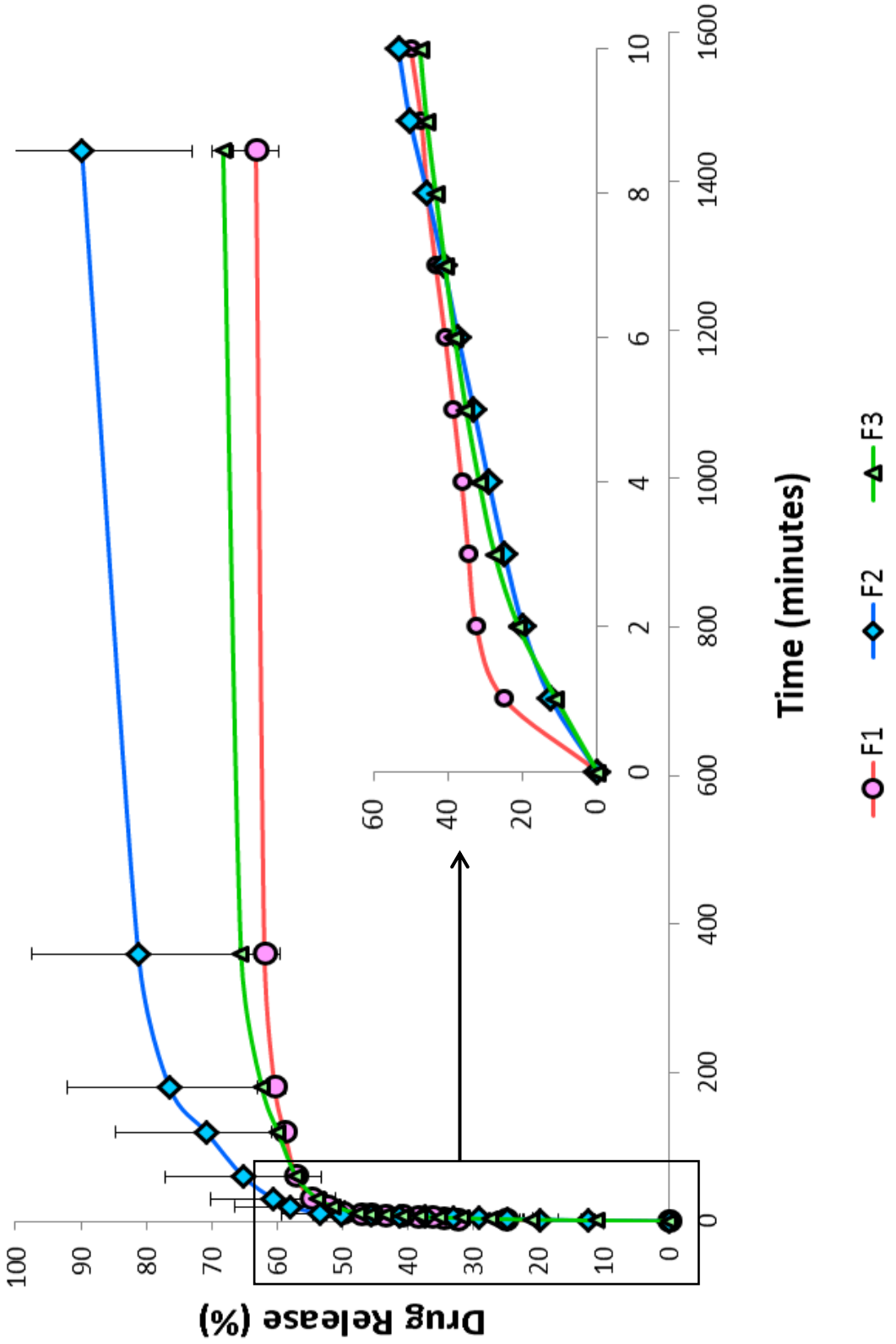

Figure 8

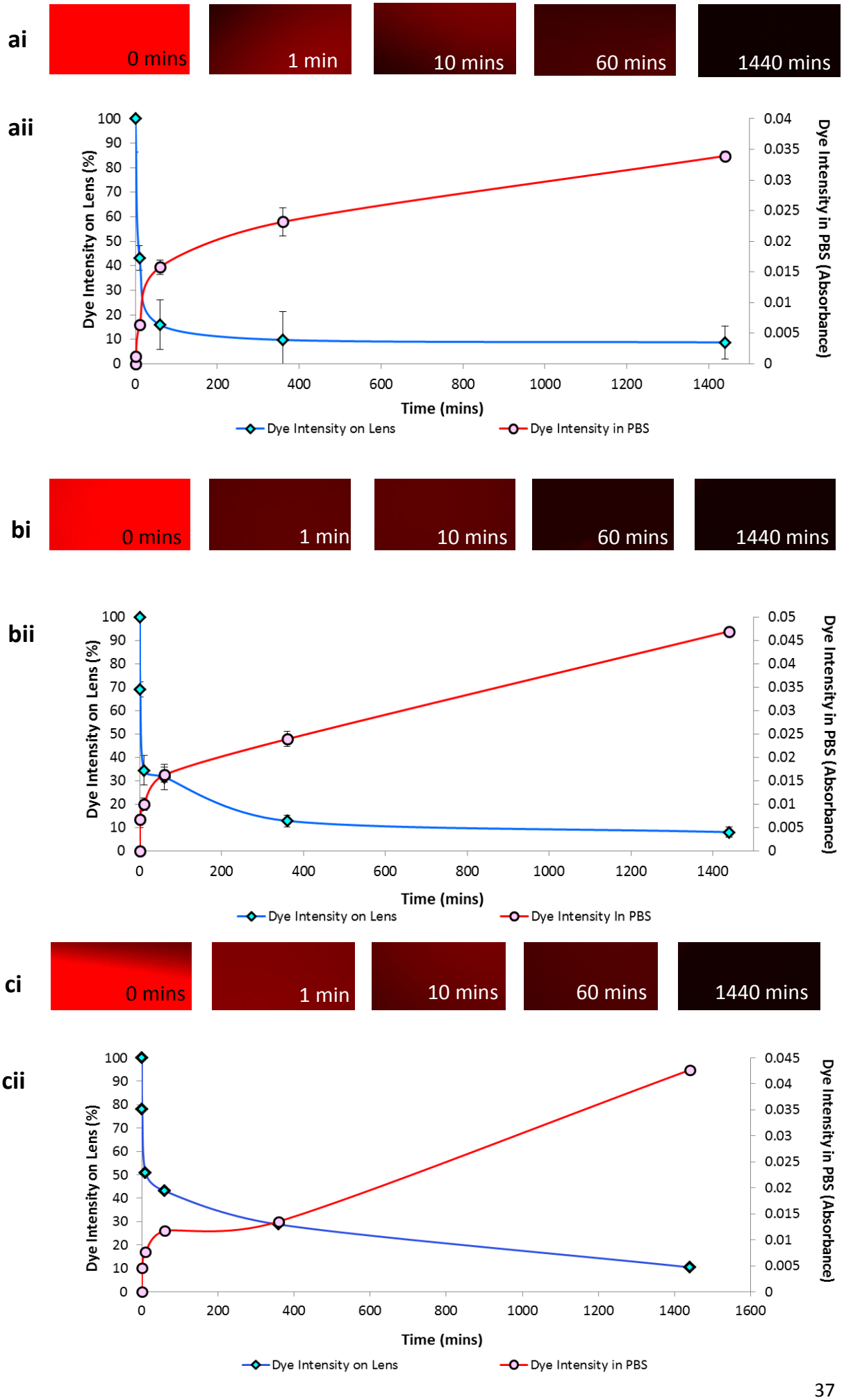
ai
0 mins
1 min
10 mins
60 mins
1440 mins
aii
Dye Intensity on Lens (%)
Dye Intensity in PBS (Absorbance)
Time (mins)
Dye Intensity on Lens
Dye Intensity in PBS
bi
0 mins
1 min
10 mins
60 mins
1440 mins
bii
Dye Intensity on Lens (%)
Dye Intensity in PBS (Absorbance)
Time (mins)
Dye Intensity on Lens
Dye Intensity In PBS
ci
0 mins
1 min
10 mins
60 mins
1440 mins
cii
Dye Intensity on Lens (%)
Dye Intensity in PBS (Absorbance)
Time (mins)
Dye Intensity on Lens
Dye Intensity in PBS

Figure 9

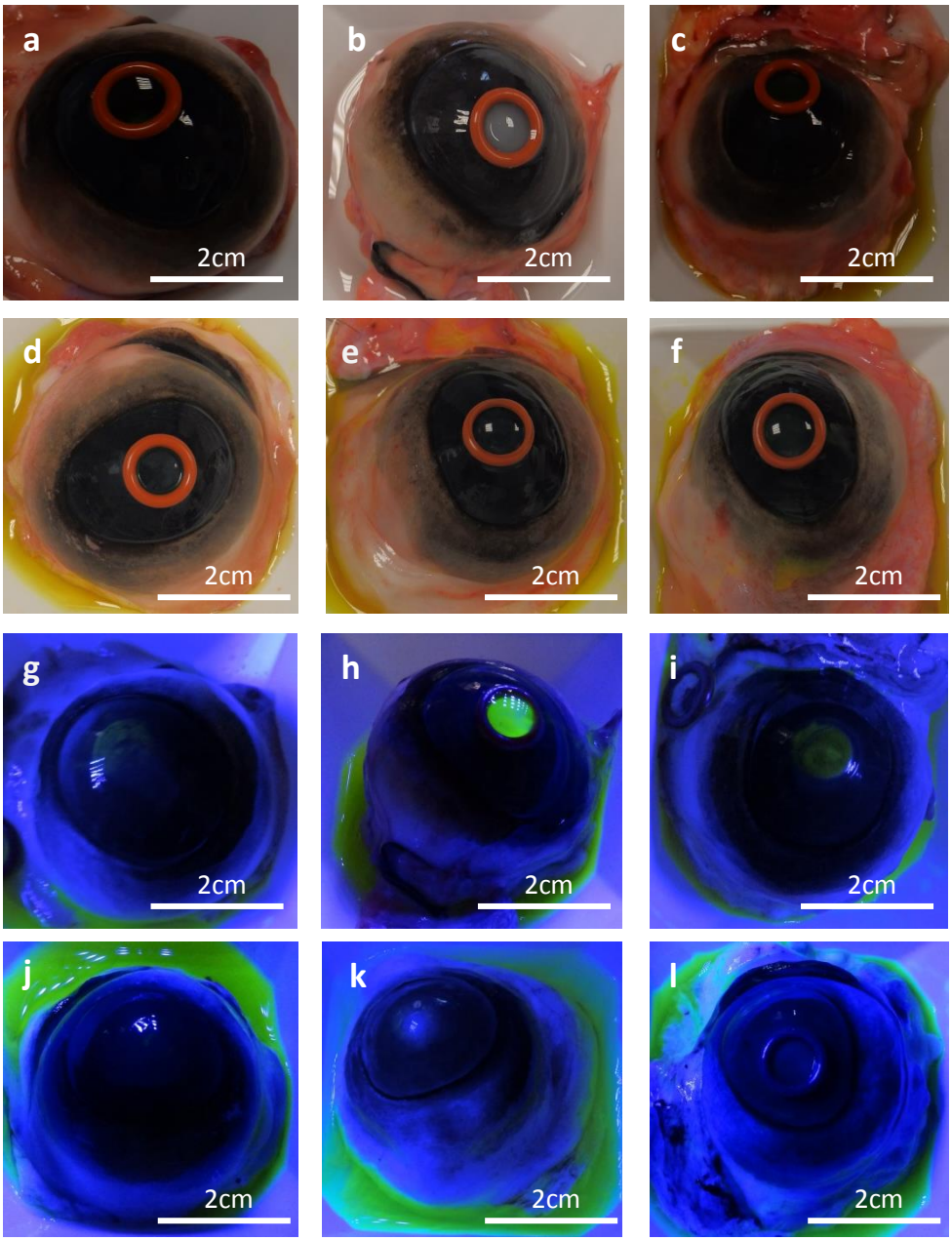

Figure 10

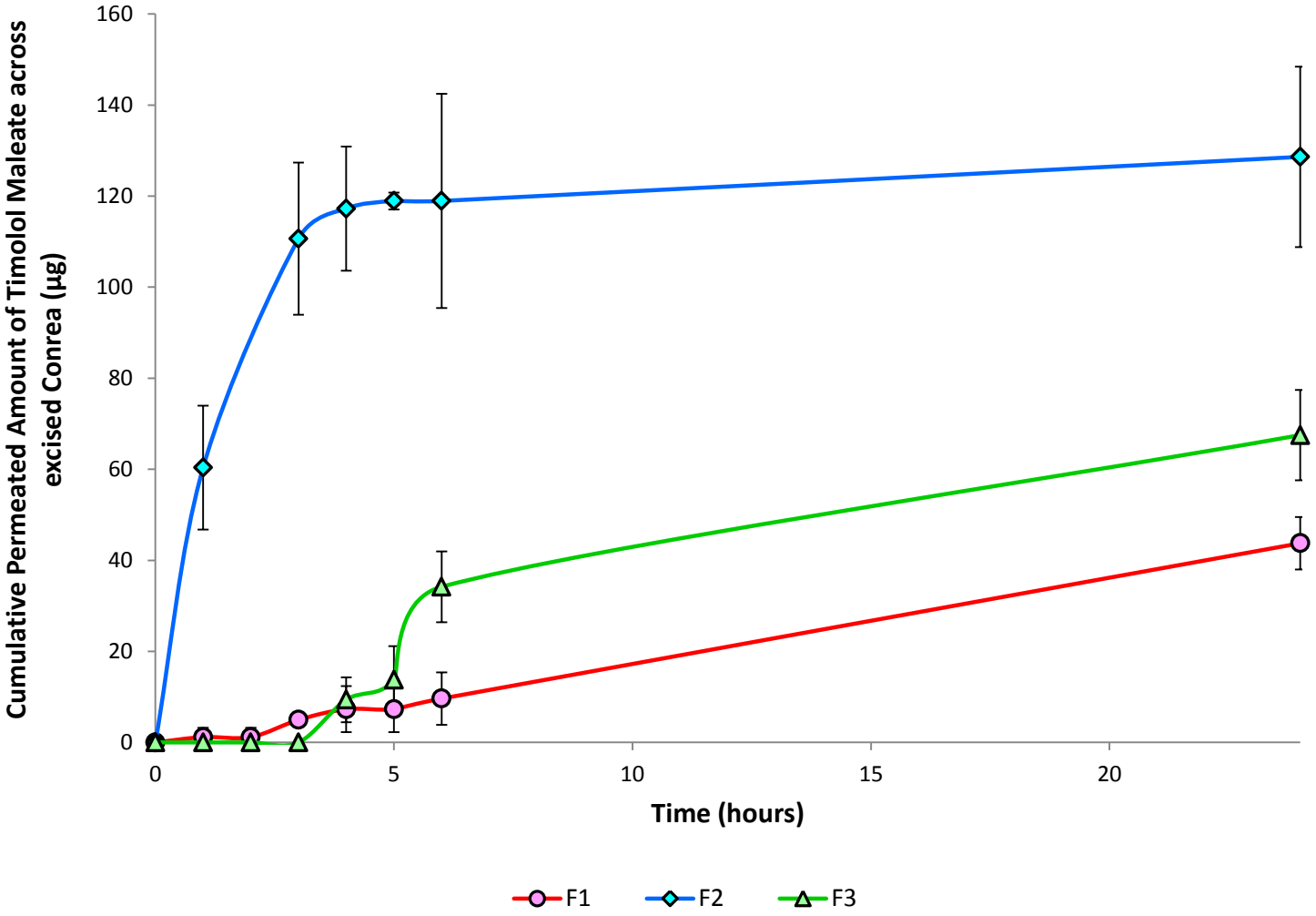
Cumulative Permeated Amount of Timolol Maleate across excised Conrea (µg)
160
140
120
100
80
60
40
20
0
0
5
10
15
20
Time (hours)
F1
F2
F3

Figure 11